PAPER • OPEN ACCESS

Emittance self-compensation in blow-out mode

To cite this article: Georgii Shamuilov *et al* 2022 *New J. Phys.* **24** 123008

View the article online for updates and enhancements.

PAPER

Emittance self-compensation in blow-out mode

Georgii Shamuilov[1] , Anatoliy Opanasenko[2], Kévin Pepitone[1] , Zoltán Tibai[3]
and Vitaliy Goryashko[1,*]

1 FREIA Laboratory, Uppsala University, Lägerhyddsvägen 1, Uppsala 75120, Sweden
2 National Science Center 'Kharkiv Institute of Physics and Technology', Akademichna 1, Kharkiv 61108, Ukraine
3 Institute of Physics, University of Pécs, Pécs 7624, Hungary
* Author to whom any correspondence should be addressed.

E-mail: vitaliy.goryashko@physics.uu.se

Abstract

We report an unusual regime of emittance self-compensation in an electron bunch generated in the blow-out mode by a radio-frequency photocathode gun. This regime is observed for a strong space-charge field on the cathode reaching around 30%–35% of the accelerating field. Simulations clearly show an initial growth and a subsequent self-compensation of projected emittance in a divergent electron bunch originating from the effects of: (a) strong space-charge forces of mirror charges on the cathode, (b) an energy chirp in the bunch and (c) substantial re-shaping of the electron bunch. Furthermore, we show analytically and numerically how a complex interplay between these effects leads to emittance self-compensation at the gun exit—the effect that is normally observed only in the presence of focusing fields.

Our progress in modern science is increasingly relying on our capability of measuring ultrafast processes on the atomic scale. Short bursts of electrons and x-rays provide the complementary ability to map the atomic structure and electronic properties of molecules, materials and nanodevices. The hard x-ray free-electron laser (XFEL) provides picometre spatial and attosecond temporal resolution for studying charge transfer in molecules, radiation damage in biomolecules, electron dynamics in chemical bonds and electron tunnelling during photoemission [1–6]. Complementary, ultrashort electron pulses offer a unique opportunity to measure the structure and dynamics of energy transformations and transport with atomic resolution as it is demonstrated with SLAC Mega electronvolt Ultrafast Electron Diffraction Instrument (MeV UED) [7] and at other UED facilities [8, 9]. Both the XFEL and MeV UED rely on high-brightness electron bunches to either directly probe samples in question via electron diffraction or to produce x-ray flashes of light to interrogate matter at extreme time and space scales. In this paper, we demonstrate a new approach to the generation of high-brightness electron bunches for applications in compact XFEL [10, 11] and UED sources [12, 13]. The proposed approach is a special regime of the blow-out mode and is well suited for the generation of ellipsoidal electron bunches at a high repetition rate.

The brightness of an electron beam, defined as the number of particles per unit volume of the total phase space [14], is the key measure of the beam quality. The main obstacle for achieving a higher brightness is the space-charge force arising in tightly packed electron bunches. The space-charge force in an ellipsoidal electron bunch with a uniform density distribution changes linearly in the bunch in any direction. Because of this nature of the space-charge force, there is no emittance growth associated with it. Such a bunch is an ideal object in accelerator physics [15]. Luiten *et al* [16] developed further the original idea of Serafini [17] and proposed a simple method for the formation of ellipsoidal electron bunches with a uniform density distribution. In the method, demonstrated experimentally for the first time by Musumeci *et al* [18], an initially short, pancake-like bunch expands to a fully-fledged uniformly charged ellipsoidal bunch thanks to its space-charge force, similarly to blowing out soap bubbles. Hence, the method is named as the blow-out mode. The initial density distribution in the bunch must have a half-circular profile in the radial direction whereas in the longitudinal direction the distribution can be arbitrary as long as the bunch is short enough. Mathematically, the required initial bunch distribution has the form $f(s)\sqrt{1 - r^2/R^2}$, where $f(s)$ is the

distribution along the longitudinal bunch coordinate s, and $\sqrt{1 - r^2/R^2}$ describes the transverse distribution with R being the *centre-to-edge* distance.

Furthermore, J. Luiten and co-workers found that the desired uniform ellipsoidal distribution is formed when the accelerating field E_{acc} is much larger than the space-charge field of the image charge induced on the cathode, i.e. $|E_{acc}| \gg |\Sigma|/\epsilon_0$. Here, Σ is the surface charge density of the bunch and ε_0 is vacuum permittivity. Under this condition, the transformation of the initial pancake bunch into an ellipsoidal one is compatible with an emittance compensation scheme [19].

The goal of our study was to find the conditions for the maximum 4D brightness in the blow-out mode, which implies the minimum normalised transverse emittance. The advantage of the blow-out mode stems from three factors:

- there is no need for special temporal laser pulse shaping, which makes the drive laser system simpler compared to other modes [16, 20];
- the microbunching instability is less severe compared to the situation when a long cylindrical bunch is produced via stacking of laser pulses [21];
- uniformly charged ellipsoidal bunches allow for excellent compressibility [10, 22].

Overall, the blow-out mode allows the realisation of high 5D brightness [20] even though the transverse emittance is not always the lowest [23]. In the specific example of the APEX-like gun studied below the blow-out regime turns out superior to the case of uniform cylindrical bunches.

In what follows, by the transverse emittance we always mean the transverse normalised root-mean-square (rms) emittance defined, e.g. in the x direction, as

$$\varepsilon_x = \frac{1}{mc} \sqrt{\sigma_x^2\, \sigma_{p_x}^2 - \text{cov}^2(x, p_x)}, \tag{1}$$

with m and c being the mass of the electron and the speed of charge, correspondingly; x and p_x are the position and momentum in the x direction; σ_x and σ_{p_x} are the standard deviations of the position and momentum, and $\text{cov}(x, p_x)$ is the covariance of x and p_x.

Our extensive numerical simulations show that the *lowest emittance for a given charge* is achieved when the space-charge field is around 35% of the accelerating one, i.e. $E_{sp-ch} \approx 0.35 E_{acc}$. Furthermore, we found that in this regime of a strong space-charge force, natural self-compensation of bunch emittance occurs. The unusual feature of this emittance self-compensation is that it occurs in a divergent electron bunch without any RF or magnetic components apart from the RF gun itself. This finding is opposite to what is known about classical emittance compensation [19, 24–27]. Note that the desired uniform ellipsoidal distribution can be simultaneously achieved.

Figure 1 reports the results of massive simulations for the emittance of an electron beam generated in blow-out mode in an APEX-like [28] continuous wave radio-frequency gun operated at 325 MHz with a peak accelerating field of 35 MV m^{-1}. The bunches are accelerated on crest to an energy of 420 keV. The bunch parameters on the cathode for an optimal regime are reported in table 1. Note that the results were independently cross-checked using three different codes: ASTRA, GPT and RFtrack. The discrepancy between the results is less than 5% and below the results from ASTRA simulations are shown.

In the simulations, starting from the Fermi–Dirac distribution of electrons in a copper cathode, electron bunches are ejected from the cathode via photo-emission using the model from [29]. The initial electron bunch distribution has the form required for the blow-out mode $\exp(-t^2/2\sigma_t^2)\,\sqrt{1 - r^2/R^2}$, where σ_t is the initial *rms* duration of the electron bunch and R is the *centre-to-edge* distance. From the Fermi–Dirac distribution, the calculated thermal emittance per unit length is 0.44 mm·mrad mm^{-1}—the value demonstrated experimentally [30, 31]. After the emission, the electron bunches move solely in the RF field of the gun, *no solenoid is present*. The laser pulse energy allows for extraction of 16 pC charge if the space-charge field is neglected. The initial electron bunch radius and duration are scanned in a wide range of parameters, even for such small radii that the electron emission is suppressed by the space-charge force. The minimum critical radius R allowing for full extraction of 16 pC corresponds to around 130 μm. In this critical regime, the accelerating field is fully screened by the space-charge field E_{sp-ch}. In analytical calculations, E_{sp-ch} is estimated as $1.17Q/(\varepsilon_0 \pi R^2)$, see [32].

Figure 1 shows a clear minimum of the emittance for the bunch duration of 30 fs (shortest duration in the simulations) and the bunch radius of around 220 μm. The resulting lowest emittance ε_{min} for the 16 pC extracted bunch is 25% above the thermal level. In this optimum scenario, the longitudinal space-charge force (accounting for the image charge on the cathode) is around 35% of the accelerating field, which is an unexpectedly high ratio. Importantly, for a given charge the obtained ε_{min} is around 40% smaller than the emittance obtained in the blow-out mode of a weak space-charge force ($E_{acc} \approx 10\,\Sigma/\epsilon_0$). Note that in each
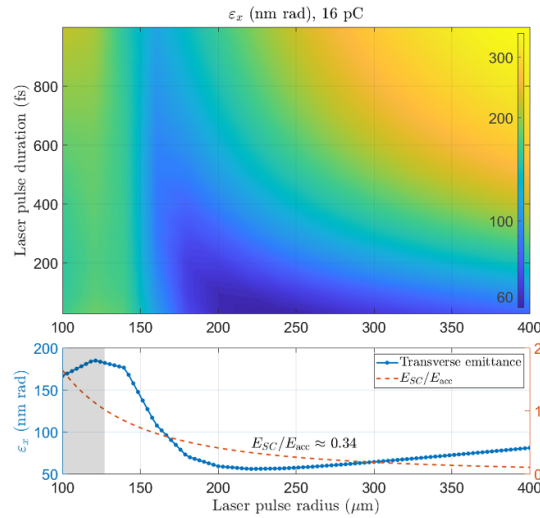
Figure 1. Upper plot: colour map of emittance as a function of the initial *rms* bunch duration (changes from 30 fs to 1 ps) and bunch radius R (note that R is the *centre-to-edge distance*; for an ellipsoidal bunch, $\sigma_x = R/\sqrt{5}$). Bottom plot: emittance (left ordinate axis) and E_{SC}/E_{acc} (right ordinate axis) as a function of R for the initial rms duration of 30 fs. The space-charge field on the cathode is estimated as $E_{SC} = \Sigma/\epsilon_0$. For $R < 130\ \mu$m, the shaded area on the left, less than 16 pC of charge is extracted because of the formation of the virtual cathode due to the strong longitudinal space-charge force eE_{SC}.

Table 1. Optimal bunch parameters on the cathode. For an ellipsoidal bunch, the rms size σ_x is connected to the radius R as $\sigma_x = R/\sqrt{5}$.

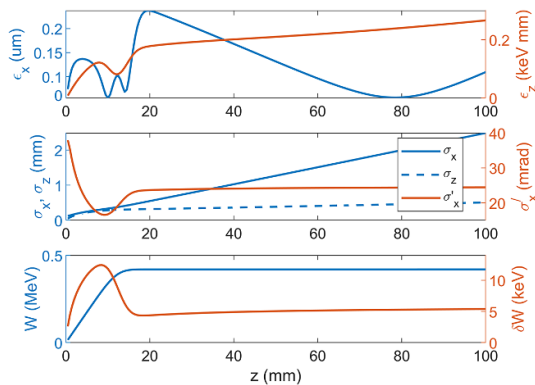| Parameter	Symbol	Value	Units
Peak accelerating field	E_{acc}	35	MV m^{-1}
Emission phase	—	0	degrees
Charge	Q	16	pC
Energy	W	130	meV
Energy spread	δW	80	meV
rms x-bunch size	σ_x	107	μm
rms bunch duration	σ_t	30	fs
rms x-beam divergence	σ_x'	2.47	mrad
rms thermal x-emittance	ε_x	44	nm

Figure 2. Evolution of the bunch parameters: the bunch transverse and longitudinal emittance ϵ_x and ϵ_z; the transverse and longitudinal bunch size σ_x and σ_z; divergence σ_x', the bunch energy W and its spread δW.

simulation run, the emittance is recorded as a function of distance from the cathode, and then, the smallest value is plotted in figure 1. Hence, in each simulation run, the optimum distance from the cathode is somewhat different but stays approximately 80 mm.

For the optimum regime, the evolution of the bunch parameters along the symmetry axis of the gun is shown in figure 2. After several oscillations, the emittance naturally attains its lowest value at 79 mm away from the cathode. The resulting bunch parameters in the optimum position are summarised in table 2.

The evolution of the transverse emittance is unusual as there are no focusing elements and an emittance compensation in the gun and after it occurs naturally. We stress that the self-aligning of the slices and the

Table 2. Beam parameters in free space after the gun at 79 mm from the cathode.

Parameter	Symbol	Value	Units
Charge	Q	16	pC
Energy	W	420	keV
Correlated energy spread	δW	5.3	keV
rms x-beam size	σ_x	2	mm
rms z-beam size	σ_z	0.46	mm
rms x-beam divergence	σ_x'	24.4	mrad
rms normalised x-emittance	ε_x	57	nm
rms normalised z-emittance	ε_z	0.24	keV mm
Ratio of x and y emittances		0.99	
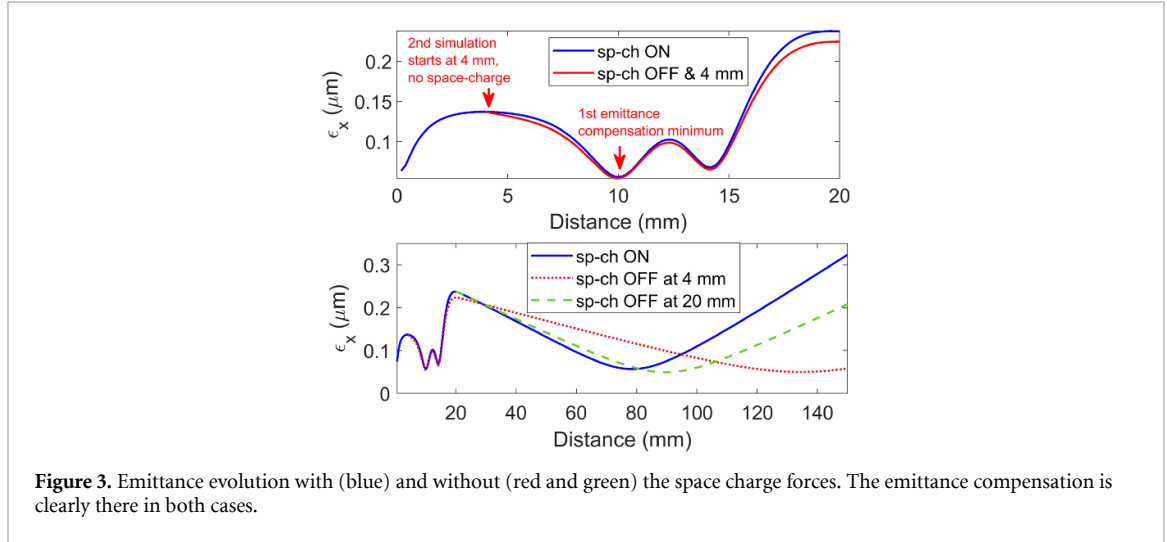
Figure 3. Emittance evolution with (blue) and without (red and green) the space charge forces. The emittance compensation is clearly there in both cases.

corresponding emittance compensation are not happening due to the space-charge field. To prove this, we run two simulation and 'switch off' space-charge forces at distances of 4 and 20 mm from the cathode, correspondingly, see figure 3. The effect of the emittance compensation is clearly seen.

Let us consider the emittance evolution in detail. The upper plot in figure 4 shows the evolution of emittance as a function of distance from the cathode and key regions which are analysed below. Figure 4 also shows a series of distributions of the transverse phase space for three slices of electrons located in the tail (blue), centre (green) and head (read) of the bunch, see the plot in the top right corner illustrating the slices used in the analysis hereinafter. We limit the analysis to the x-p_x plane thanks to the rotational symmetry of the problem. Note that in all plots *the linear correlation between x and p_x—calculated for all electrons in the bunch—is removed* to reveal the fine structure of the x-p_x distribution. Also, in all the plots the x-coordinate is shown in the units of the rms beam size σ_x calculated at each z position.

The details of the bunch dynamics are further analysed in figure 5 that reports: (a) the aspect ratio of the longitudinal to transverse bunch length, (b) the coefficients of the linear and cubic correlations between x and p_x for the three slices mentioned above. These coefficients are the result of a least-squares fit having the form $p_x = p_0 + p_1(x/\sigma_x) + p_3(x/\sigma_x)^3$.
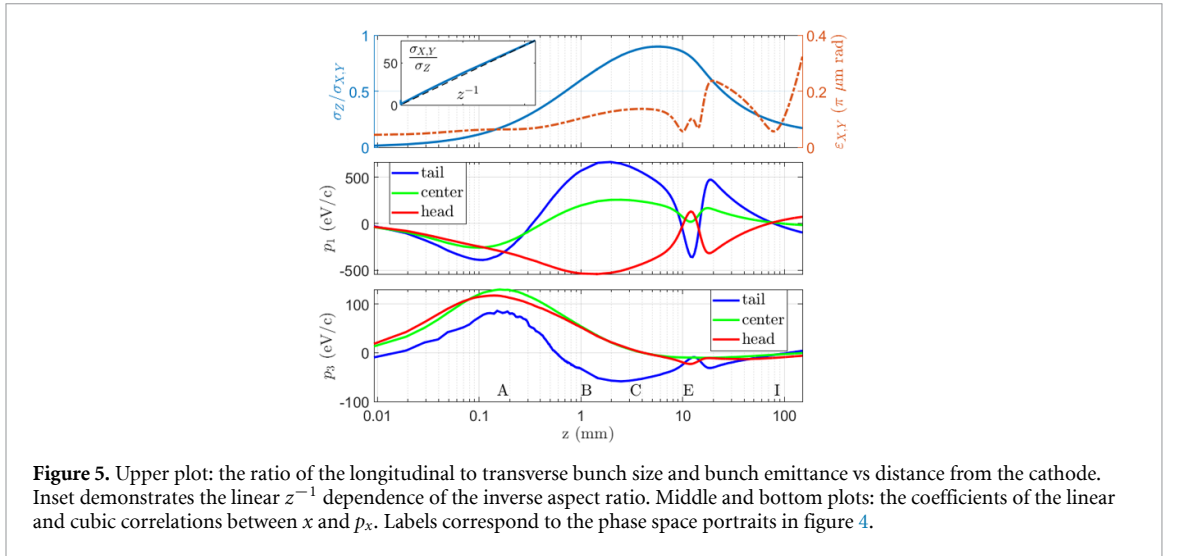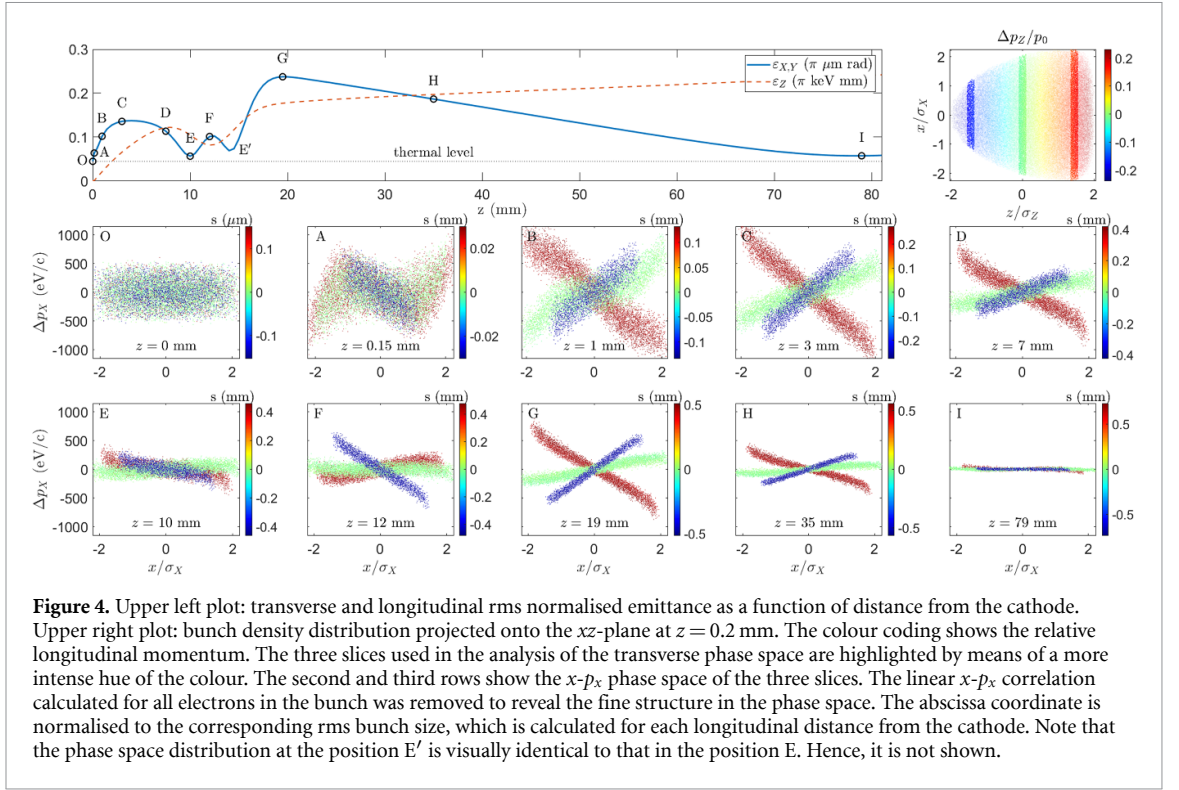
Let us examine in detail the evolution of emittance in figure 4 step-by-step and we start with considering the region OA. In this region, the total space-charge field is given by the superposition of the space-charge field of the bunch itself and its mirror charge on the cathode. The radial component of the space-charge field reads

$$E_r = -\frac{\partial}{\partial r}(\varphi_- + \varphi_+), \quad \varphi_\pm = \frac{1}{4\pi\epsilon_0} \int \frac{\varrho_\pm dV'}{|\vec{r} - \vec{r}'|}, \tag{2}$$

where $\varrho_\pm = \pm\Sigma\sqrt{1 - r^2/R^2}\delta(z \pm z_b)$ is the initial bunch density. The bunch is assumed to be infinitesimally thin and located at z_b. By Taylor expanding E_r into the powers of the radial distance r, one obtains the linear and cubic component of E_r.

Let us start from the *cubic term* having the form

$$E_r^{\text{cubic,OA}} = \frac{\Sigma}{2\epsilon_0} \frac{\zeta_b \rho^3}{(1 + 4\zeta_b^2)^3}, \tag{3}$$

Figure 4. Upper left plot: transverse and longitudinal rms normalised emittance as a function of distance from the cathode. Upper right plot: bunch density distribution projected onto the *xz*-plane at $z = 0.2$ mm. The colour coding shows the relative longitudinal momentum. The three slices used in the analysis of the transverse phase space are highlighted by means of a more intense hue of the colour. The second and third rows show the x-p_x phase space of the three slices. The linear x-p_x correlation calculated for all electrons in the bunch was removed to reveal the fine structure in the phase space. The abscissa coordinate is normalised to the corresponding rms bunch size, which is calculated for each longitudinal distance from the cathode. Note that the phase space distribution at the position E$'$ is visually identical to that in the position E. Hence, it is not shown.

Figure 5. Upper plot: the ratio of the longitudinal to transverse bunch size and bunch emittance vs distance from the cathode. Inset demonstrates the linear z^{-1} dependence of the inverse aspect ratio. Middle and bottom plots: the coefficients of the linear and cubic correlations between x and p_x. Labels correspond to the phase space portraits in figure 4.

where $\zeta_b = z_b/R$ and $\rho = r/R$ are the normalised longitudinal bunch position and radial coordinate, respectively. The cubic non-linearity of E_r gives rise to an emittance increase in the region OA, see plot A in figure 4 and also the plot of p_3 in figure 5. The maximum of $E_r^{\text{cubic,OA}}$ is reached for $z_b^{\text{cr}} = 1/(2\sqrt{5})R \approx 0.2R$. For our simulation parameters, $z_b^{\text{cr}} \approx 50\,\mu$m and at this position the gradient of the fit coefficient p_3 attains its maximum value. Recall that the shape of the transverse phase space is the result of the cumulative action of E_r (the radial component of the accelerating field is uniform in the gun region except for the output aperture). Hence, $dp_3/dz \propto E_r^{\text{cubic}}/v_z$, where v_z is the longitudinal velocity. The nonlinear emittance growth in the cathode region for cylindrical bunches was also studied before in [33]. The rf-induced emittance growth calculated using the Floettmann model [34] is 6.7 pm. The very long RF period (3 ns) makes the rf-induced emittance negligible.

To illustrate the analytical estimates, in figure 6 we show the radial electric field of the bunch and its image charge for different distances from the cathode. The plots are extracted from the ASTRA simulations and the result of self-consistent dynamics of the electrons and the fields. The distribution of E_r is *highly nonlinear near the cathode but quickly linearises as the bunch expands*, reshapes and the effect of the image charge diminishes with distance. For $z > R$, the E_r distribution is primarily linear.
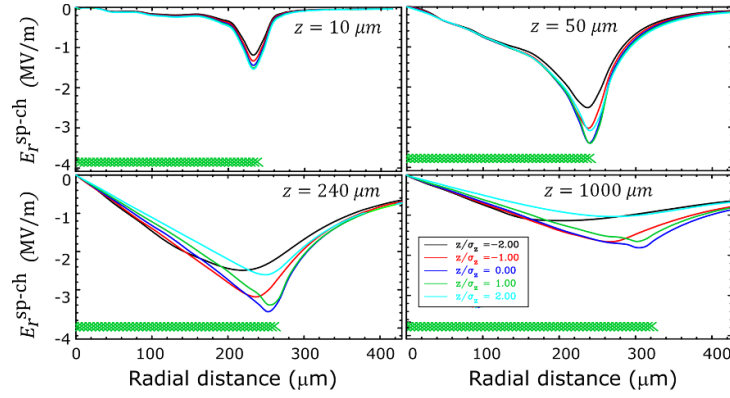
Figure 6. Radial component of the space-charge field taking into account the image charge vs radial distance for 5 slices of the beam. Near the cathode, E_r has an essentially nonlinear dependence on r but as the bunch blows out and the charge density becomes more uniform, E_r distribution becomes more linear. Note the change in the sign of the curvature, cf E_r at 10 and 1000 μm from the cathode. This change of the curvature leads to the linearisation of the phase-space of the bunch. The green rectangular shows the longitudinal extent of the bunch.
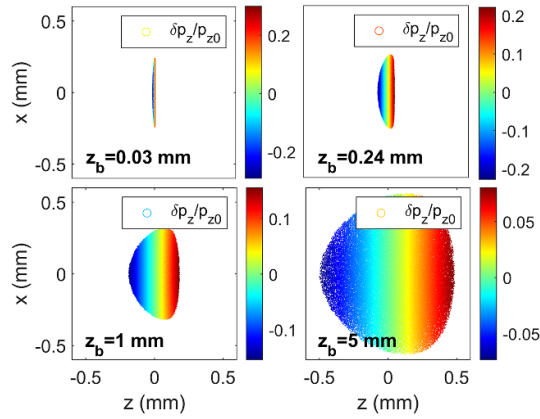

Figure 7. Expansion of the pancake bunch as it flies from the cathode. The colour coding shows the relative longitudinal momentum of the electrons. At distances $z < R$ the bunch expands primarily in the longitudinal direction due to a very strong energy chirp created by a strong longitudinal space-charge field. After $z > R$, the bunch expands both longitudinally and transversely.

In the region AB, two effects occur: (a) the transverse phase-space self-linearises and (b) emittance grows because of relative rotation (misalignment) of the slices due to different magnitudes of the radial component of the linear space-charge force along the bunch. Namely, for $z_b > R/2$ the radial space-charge field E_r is mostly due to the field of the bunch itself and the cubic component might be *estimated* as

$$E_r^{\text{cubic,AB}} = -\frac{\Sigma}{\epsilon_0}\,\zeta_l^2\,\rho^3, \tag{4}$$

where $\zeta_l = \sigma_z/R$ is the normalised bunch length. The bunch is not infinitesimally thin anymore because of its expansion. Note that now $E_r^{\text{cubic,AB}}$ has a different sign compared to that in the region OA and counteracts the effect of the phase-space non-linearity induced before. The change in the sign of the curvature of E_r is clearly seen in figure 6. As a result, one can see from figure 5 that the non-linear component of the phase space distribution almost completely disappears after a few mm from the cathode thanks to the compensation. Appreciate almost linear phase space distributions in the plots A-I of figure 4.

Now, we turn our attention to the relative motion of electron slices due to the linear component of E_r. First, very near the cathode, $z_b \ll R$, all electrons experience the same linear space-charge field $E_r^{\text{lin}} = (\Sigma/\epsilon_0)(z_b r/R^2)$, see the first plot in figure 6. Hence, all slices get the same transverse kick as it can also be seen from the plot of p_1 in figure 5. Note that the image charge gives a focusing effect and $E_r^{\text{lin}} = 0$ for the bunch being just on the cathode, $z_b = 0$.

As the bunch flies away and expands in the region OA, it takes an egg-like shape, see the top right plot in figure 7, primarily because of the pulling effect of the longitudinal space-charge force of the image charge on the cathode. A head-tail energy correlation—called energy chirp—develops due to the longitudinal
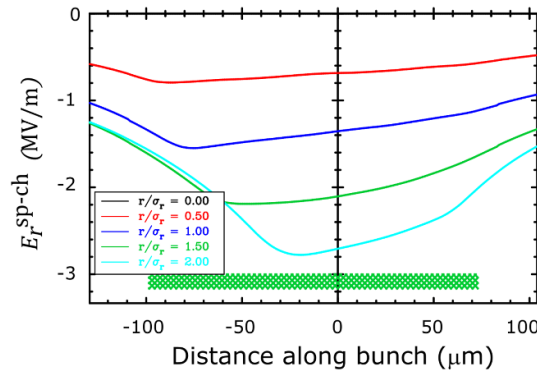
Figure 8. Distribution of the radial space-charge force along the bunch. The field acting on the tail is almost 30% stronger than the one acting on the head. At a distance 1 mm from the cathode.

space-charge force. There is also a weak focusing force in the radial direction due to the image charge. For the tail, this focusing is stronger than for the head simply because of the shorter distance to the cathode.

In the region AC, $z > R/2$, the transverse bunch dynamics is dominated by its own linear space-charge field and different slices acquire different amounts of x-p_x correlation, see plots B and C in figure 4, and the plot for p_1 in figure 5.

The difference in the magnitude of the correlations for the tail and head slices (in other words, the tilt angles of the slices in the phase space) is due to the acquired momentum $\Delta p_r \propto E_r^{\text{lin}} \Delta t$ that changes linearly along the bunch because there is a gradient of E_r^{lin} along the bunch. This longitudinal gradient of E_r^{lin} for a fixed r is illustrated in figure 8.

The difference in defocusing strength leads to a relative rotation between the slices in the $x - p_x$ plane. Simultaneously, as the bunch dynamics evolves further, the egg-like shape transforms into a proper ellipsoidal shape, see figure 7, because the tail expands faster than the head due to tail's larger divergence. The field E_r^{lin} becomes constant along the bunch. By the end of the region AC, the bunch density drops by 2 orders of magnitude because of bunch expansion.

Between the positions C and E, see figure 4, the bunch aspect ratio remains approximately constant, see the upper plot in figure 5, whereas the bunch shape is nearly ellipsoidal. In this region, the projected emittance reduces almost to the thermal value as the *tail slices rotate towards the head slices* in the phase space due to the larger correlation in the tail.

To understand better the self-aligning of the slices, consider two electrons having the same x-coordinate but located in the tail, superscript t, and in the head, superscript h. As seen from figures 4 and 8, the moment of the tail p_x^t is larger than that of the head p_x^h, $p_x^t > p_x^h$. After propagating a distance l, the separation between the electrons can be estimated in the ballistic approximation as $l(p_x^t - p_x^h)/p_z^{\text{ref}}$, where p_z^{ref} is the longitudinal momentum of the reference particle. The difference is negative and the tail electron catches up with head one, compare also with an analytical model of chromatic emittance variation by Floettmann [34]. Note that the linear nature of the gradient of E_r along the bunch, i.e. $\partial E_r / \partial s \propto \text{const}$, allows for a complete emittance compensation.

The region EG corresponds to a transition through the gun exit aperture. A clear and simple treatment of the radial bunch dynamics in the transition region can be found in the Wangler book [35]. The *resulting transverse momentum change* can be estimated as $\Delta p_r = eE_{\text{acc}}r/2\bar{v}_z$, where $\bar{v}_z$ is the average longitudinal velocity v_z in the exit aperture region. Because of the head-tail energy chirp ($v_z^h > v_z^t$), the tail electrons acquire a larger transverse kick and the tail slice is rotated counter-clockwise with respect to the head slice, see the plot G in figure 4. The emittance peaks at the exit of the aperture.

The emittance oscillation between the points E and E' is due to the gradient of E_{acc} and is a local effect that has no impact on subsequent emittance evolution. The effect of the RF-induced emittance growth in the gun aperture can be singled out by running simulations without space-charge as demonstrated in figure 9.

We also note that the energy chirp has two components: (a) one due to the space-charge force, and (b) the other one due to the accelerating RF field. The second contribution to the chirp collapses almost to zero when the bunch leaves the cavity.

In the region GI, the tail slices catch up with the head slices due to a larger rotation speed proportional to p_x/p_z. It is the same mechanism as in the region CE discussed in details above.

The linear mechanism of the growth and self-compensation of the projected emittance can be summarised as follows: (a) quick misalignment of the tail and head slices due to the longitudinal gradient of the space-charge force in the cathode region or a relative kick from the accelerating field in the exit aperture
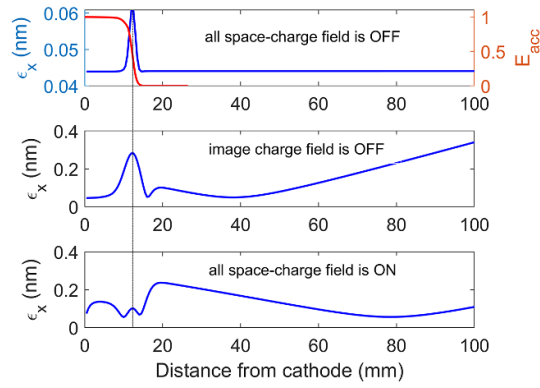
Figure 9. Evolution of the bunch emittance for different simulation scenarios. The top plot shows the evolution of emittance without any space-charge fields. In this special case, the initial bunch length is 1 ps to make this scenario consistent with the case when space-charge fields are accounted for and the bunch expands. If the bunch were ultrashort, no RF-induced effect would be noticeable as all slices 'see' the same radial field E_r in the aperture.
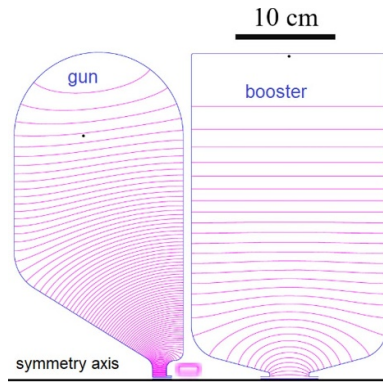

Figure 10. Geometry of an injector composed of the gun, a normal conducting booster and a small solenoid in between.
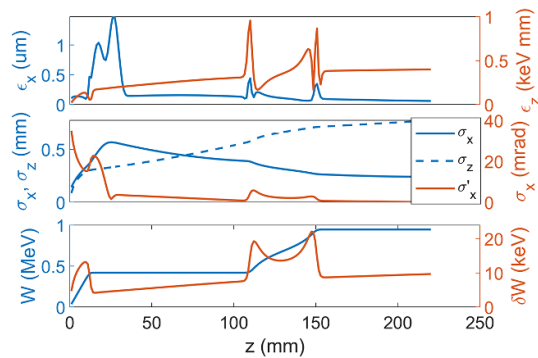

Figure 11. Evolution of the bunch parameters in the injector using the blow-out regime of the gun.

because of the energy chirp; (b) slow self-alignment of the slices due to the ballistic effect. These two processes can be thought of as some excitation-relaxation mechanism which occurs twice: in the gun (regions AC and CE) and in the exit aperture followed by drift space (regions E'G and GI).

The discovered regime allows generating bunches with the *lowest possible emittance for a given charge in an APEX-like RF gun with a moderate accelerating field*. As an example, we tracked the studied above bunch distribution through a 325 MHz normal conducting booster and found the emittance to be preserved on a 60 nm scale for 16 pC bunches. A small solenoid at the gun exit is added to focus the bunch into the 325 MHz booster operated on crest. The geometry is shown in figure 10 and the evolution of bunch parameters is presented in figure 11.

For comparison, we also made a quick optimisation study of beam parameters in the regime of long uniform cylindrical bunches. The critical current and the corresponding bunch duration for a charge of 16

Table 3. Comparison of the beam parameters on the cathode for three distributions. For the flattop distribution the pulse duration is specified as an edge-to-edge duration* whereas for the Gaussian distribution it is an rms value.

Bunch shape	Cylindric	Cylindric	Ellipsoidal
Transverse distribution	Uniform	Uniform	Parabolic
Centre-to-edge radius (μm)	130	240	240
x-emittance (μm)	0.027	0.048	0.044
Temporal distribution	Flattop	Flattop	Gaussian
Pulse duration (ps)	6.3*	2.5 *	0.03

Table 4. Comparison of the beam parameters at the exit of the injector (0.95 MeV beam energy) for three distributions.

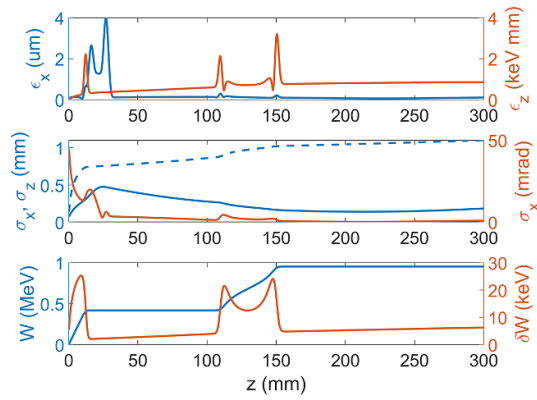| Bunch shape	Cylindric	Cylindric	Ellipsoidal
Energy spread (keV)	5.5	9	9.7
x-emittance (μm)	0.07	0.1	0.06
z-emittance (keV mm)	0.82	0.5	0.4
rms beam radius (mm)	0.14	0.27	0.24
rms beam divergence (mrad)	0.2	0.72	0.09
rms beam length (mm)	1.05	0.8	0.77

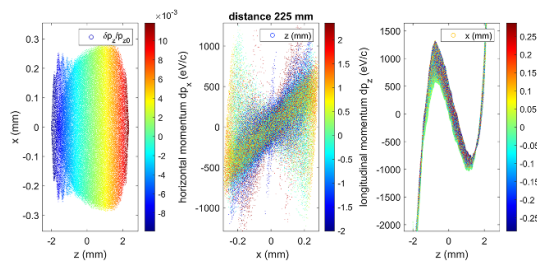**Figure 12.** Evolution of the parameters of a *uniform cylindrical* bunch in the injector.

Figure 13. Phase space for the 130 μm *uniform cylindrical* bunch after the injector. From left to right: (i) bunch distribution in the *x-z* coordinates with the colour indicating the relative longitudinal momentum; (ii) x-p_x phase space with the colour indicating the longitudinal position in the bunch; (iii) z-p_z phase space with the colour indicating the transverse position in the bunch.

pC are calculated from [36]. We considered two cases with a centre-to-edge radius of 130 μm and 240 μm. The initial and final parameters are summarised in the tables 3 and 4. The evolution of the beam parameters for the 130 μm case is shown in figure 12. The 6D brightness is two times larger in the blow-out regime compared to the regime of thin cylindrical bunches. While long uniform bunches can have a much smaller initial emittance, the final emittance is even larger than in the blow-out mode despite optimisation. The reason for a large transverse emittance is non-linear space-charge forces at the bunch edge (see figure 2 in the [27]), which cause a nonlinear deformation of phase space, see figure 13.

To sum up, the discovered regime of emittance self-compensation is observed in a wide range of bunch charges from 160 fC to 16 pC. This regime is also observed for different lengths of the accelerating gun region deliberately designed to study possible limitations. The emittance self-compensation is, in general, robust

except that the initial radial distribution of the bunch density must be close to a half-circular distribution to keep space-charge forces linear. The effect of self-compensation in blow-out mode with strong space-charge forces seems to be universal. The extent and position of self-compensation depend on specific settings of the gun.

High-brightness electron beams are crucial for UED experiments and accelerator-based light sources, and we believe that the discovered mode of operation would allow for a new level of performance for these machines.

Data availability statement

The data that support the findings of this study are available upon reasonable request from the authors.

Acknowledgment

ORCID iDs

Georgii Shamuilov ⬤ https://orcid.org/0000-0003-2697-4009
Kévin Pepitone ⬤ https://orcid.org/0000-0002-4514-293X
Zoltán Tibai ⬤ https://orcid.org/0000-0002-3196-7586
Vitaliy Goryashko ⬤ https://orcid.org/0000-0002-8217-1174

References

[1] Emma P *et al* 2010 *Nat. Photon.* **4** 641
[2] Huang Z and Lindau I 2012 *Nat. Photon.* **6** 505
[3] Ko I *et al* 2017 *Appl. Sci.* **7** 479
[4] Milne C *et al* 2017 *Appl. Sci.* **7** 720
[5] Tschentscher T, Bressler C, Grünert J, Madsen A, Mancuso A, Meyer M, Scherz A, Sinn H and Zastrau U 2017 *Appl. Sci.* **7** 592
[6] Mak A *et al* 2019 *Rep. Prog. Phys.* **82** 025901
[7] Weathersby S P *et al* 2015 *Rev. Sci. Instrum.* **86** 073702
[8] Chatelain R P, Morrison V R, Godbout C and Siwick B J 2012 *Appl. Phys. Lett.* **101** 081901
[9] Giret Y, Naruse N, Daraszewicz S L, Murooka Y, Yang J, Duffy D M, Shluger A L and Tanimura K 2013 *Appl. Phys. Lett.* **103** 253107
[10] Nanni E, Graves W and Moncton D 2018 *Phys. Rev. Accel. Beams* **21** 014401
[11] Rosenzweig J B *et al* 2020 *New J. Phys.* **22** 093067
[12] Sciaini G and Miller R J D 2011 *Rep. Prog. Phys.* **74** 096101
[13] Miller R J D 2014 *Annu. Rev. Phys. Chem.* **65** 583
[14] Bazarov I V, Dunham B M and Sinclair C K 2009 *Phys. Rev. Lett.* **102** 104801
[15] Reiser M 2008 *Theory and Design of Charged Particle Beams* (New York: Wiley)
[16] Luiten O J, van der Geer S B, de Loos M J, Kiewiet F B and van der Wiel M J 2004 *Phys. Rev. Lett.* **93** 094802
[17] Serafini L 1994 *Nucl. Instrum. Methods Phys. Res.* A **340** 40
[18] Musumeci P, Moody J T, England R J, Rosenzweig J B and Tran T 2008 *Phys. Rev. Lett.* **100** 244801
[19] Rosenzweig J, Cook A, England R, Dunning M, Anderson S and Ferrario M 2006 *Nucl. Instrum. Methods Phys. Res.* A **557** 87
[20] Faillace L *et al* 2022 *Phys. Rev. Accel. Beams* **25** 063401
[21] Bettoni S, Divall M C, Ganter R, Pedrozzi M, Prat E, Reiche S, Schietinger T, Trisorio A, Vicario C and Goryashko V 2020 *Phys. Rev. Accel. Beams* **23** 024401
[22] van Oudheusden T, de Jong E F, van der Geer S B, 't Root W P E M O, Luiten O J and Siwick B J 2007 *J. Appl. Phys.* **102** 093501
[23] Li Y 2008 Comment on "How to realize uniform three-dimensional ellipsoidal electron bunches" (arXiv:0809.1582)
[24] Carlsten B E 1989 *Nucl. Instrum. Methods Phys. Res.* A **285** 313
[25] Carlsten B E 1995 *Part. Accel.* **49** 27 (available at: https://inspirehep.net/files/eb0cb6e4d90f32962137f5642af2af5a)
[26] Serafini L and Rosenzweig J B 1997 *Phys. Rev.* E **55** 7565
[27] Floettmann K 2017 *Phys. Rev. Accel. Beams* **20** 013401
[28] Wells R P, Ghiorso W, Staples J, Huang T M, Sannibale F and Kramasz T D 2016 *Rev. Sci. Instrum.* **87** 023302
[29] Dowell D H and Schmerge J F 2009 *Phys. Rev. ST Accel. Beams* **12** 074201
[30] Hauri C P, Ganter R, Pimpec F L, Trisorio A, Ruchert C and Braun H H 2010 *Phys. Rev. Lett.* **104** 234802
[31] Divall M C, Prat E, Bettoni S, Vicario C, Trisorio A, Schietinger T and Hauri C P 2015 *Phys. Rev. ST Accel. Beams* **18** 033401
[32] Shamuilov G, Mak A, Pepitone K and Goryashko V 2018 *Appl. Phys. Lett.* **113** 204103
[33] Cee R, Krassilnikov M, Setzer S, Weiland T and Novokhatski A 2002 *Nucl. Instrum. Methods Phys. Res.* A **483** 321
[34] Floettmann K 2015 *Phys. Rev. ST Accel. Beams* **18** 064801
[35] Wangler T P 2008 *RF Linear Accelerators* (New York: Wiley)
[36] Filippetto D, Musumeci P, Zolotorev M and Stupakov G 2014 *Phys. Rev. ST Accel. Beams* **17** 024201